Journal of Photopolymer Science and Technology
Volume 25, Number 2 (2012) 189 –196 © 2012CPST

Reactive-monolayer-assisted Thermal Nanoimprint Lithography

Shoichi Kubo[1] and Masaru Nakagawa[1,2]

[1]Institute of Multidisciplinary Research for Advanced Materials (IMRAM), Tohoku University
2-1-1 Katahira, Aoba-ku, Sendai 980-8577, Japan
[2]Core Research Evolutional Science and Technology (CREST), Japan Science and Technology Agency (JST)
7 Gobancho, Chiyoda 102-0076, Japan
nakagawa@tagen.tohoku.ac.jp

This article gives an overview of reactive-monolayer-assisted thermal nanoimprint lithography (R-TNIL) for the fabrication of patterned metal thin layers on substrates by simple wet etching using a thermoplastic polymer resist layer assisted by photochemically grafted polymer layer. A photoreactive monolayer causing a photoinduced graft reaction on the metal surface anchors interfacial resist polymers, resulting in the suppression of thermally induced dewetting of the resist layer and the improvement of lateral pattern resolution of metal thin layers. Line widths of metal patterns could be tuned by controlled side etching. Enhanced adhesion of resist layers was revealed by lateral force curves measured by scanning probe microscopy. It was demonstrated as an application that transparent conductive substrates having metal mesh structures were fabricated by R-TNIL. We also demonstrated R-TNIL involving electrodeposition, which allowed the preparation of metal patterns with controlled aspect ratio. It was proved that the photoreactive monolayer played important roles to fabricate submicrometer patterns of metal thin layers.

Key words: nanoimprint lithography, photoreactive monolayer, patterning, metal thin film, wet etching, electrodeposition

1. Introduction

Nanoimprint lithography (NIL) has attracted much attention as one of the promising nanofabrication techniques, which has a characteristic of line edge roughness at atomic resolution and capable of compensating insufficient throughput of fine electron beam (EB) lithography. The situation allows the principle study and industrial development of advanced nanostructure devices. In general, a master mold is generally made by EB lithography and subsequent dry etching. The fine nanopatterns of the mold can be replicated to multiple resin resist layers at high throughput. Thermal nanoimprint lithography (TNIL) was first proposed to transform a resist layer of thermoplastic polymers by pressing the mold above a glass transition temperature (T_g), cooling below T_g, releasing the mold from the transformed resist layer [1]. After removal of residual layers formed at concave regions of the patterned resist layer, Au/Ti dot patterns with a size of 25 nm can be fabricated by a subsequent lift-off process. Since the first report, other NIL methods have been proposed such as ultraviolet nanoimprint lithography (UV-NIL) using liquid UV-curable resins [2] and

Received April 22, 2012
Accepted May 25, 2012

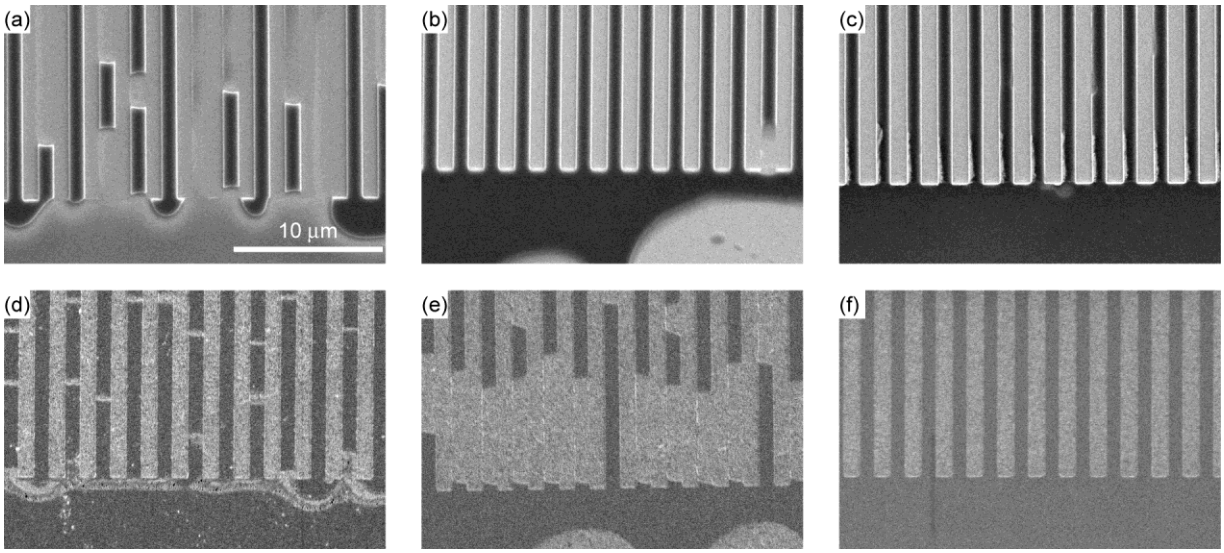

Fig. 1. SEM images of (a–c) PS resist layers thermally transformed by using a fluorinated silicon mold having 1 μm line-and space pattern and (d–f) patterned Au thin layers after removal of residual layers, Au wet etching, and removal of resist layers and PrM. The PS resist layer on (a, d) a bare Au substrate, (b, e) a PrM-modified substrate, and (c, f) a UV-exposed PrM-modified substrate with a PS graft layer was used.

room temperature nanoimprint lithography (RT-NIL) with spin-on-glass (SOG) materials [3, 4].

We demonstrated reactive-monolayer-assisted thermal nanoimprint lithography (R-TNIL) as an advanced TNIL technique [5, 6]. In R-TNIL, a surface of a metal-plated substrate is modified with a photoreactive monolayer (PrM) having a benzophenone moiety and then a resist layer of thermoplastic polymer polystyrene (PS). PS molecules near the PrM are anchored covalently to the PrM on the substrate by a photochemical graft reaction upon exposure to UV light, resulting in the suppression of thermally induced dewetting of the resist layer [7]. Due to the assistance of the polymer graft layer, lateral resolutions of transformed resist layers and metal thin layers by a simple wet etching process are greatly improved. The simple method for fabricating patterned metal thin layers by R-TNIL is considered to be applicable to electrical, optical, and magnetic devices.

In this article, we provide an overview of R-TNIL to fabricate patterned metal thin layers on substrates from the viewpoint of scientific roles that the PrM plays. We will show again the effect of the PrM on lateral patterning resolution in nanoimprint processes. Besides one-to-one replication, using an identical mold, line widths of a patterned metal thin layer could be tuned simply by changing a period of wet etching on the basis of progressive side-etching. Enhanced adhesion of an individual resist pattern prepared on the PrM-modified substrate was confirmed by an increase in lateral force during pattern collapse by scanning a probe in a direction parallel to a substrate surface. As an example of R-TNIL to practical application, we demonstrated the fabrication of transparent conductive substrates having metal mesh structures in a subtractive way. In addition, we showed an additive way using electrodeposition for the fabrication of patterned metal thin layers with controlled heights.

2. Photoreactive monolayer assisting pattern fabrication

2.1. Improvement of lateral resolutions of patterned resist and metal layers by dewetting suppression

Oda *et al.* first reported that suppression of thermally induced dewetting of a PS resist layer could be caused by exposure of the PS resist layer on a PrM-modified Au-plated substrate to UV light as a result of a photochemical graft reaction [5, 7]. The PrM is formed from 4-[(10-mercaptodecyl)oxy]-benzophenone by immersion of Au-plated substrates in its ethanol solution. Using a PS showing weight-average molecular weight (M_w) of 45,000 g mol^{-1}, the resist layer is prepared by spin coating on the PrM-modified substrate. The resist layer is exposed to UV light to cause benzophenone photochemistry. For comparison, PS resist layers on a bare Au substrate and on a PrM-modified substrate without UV-exposure are prepared. The three kinds of PS resist layer are transformed at 120 °C.

Figures 1(a–c) show scanning electron microscope (SEM) images of PS resist layers transformed to 1 μm line-and-space patterns. Many defects occur in the PS resist layer on a bare Au substrate [Fig. 1(a)] and on a PrM-modified Au substrate [Fig. 1(b)] due to thermally induced dewetting and capillary action during thermal nanoimprinting. Such

defects are hardly observed on a UV-exposed PrM-modified Au substrate [Fig. 1(c)]. The reason is considered that the formation of PS graft layer makes a surface tension of the substrate approaching to that of the PS resist layer. Figures 1(d–f) show SEM images of patterned Au layers on an adhesive Cr layer of a silicon substrate prepared by Au wet etching. The wet etching is performed after removal of a residual layer formed at concave regions of the PS resist layer by exposure to UV/ozone. The number of defect in patterned Au layers is obviously increased in the case of the PrM-modified Au substrate without UV-exposure [Fig. 1(e)]. The comparison with the case of the UV-exposed PS resist layer on the PrM-modified Au substrate [Fig. 1(f)] clearly indicates that physical adhesion of the unexposed PS resist layer to the PrM-modified Au substrate is so weak that penetration of an aqueous wet etchant into an interface between the PS resist layer and PrM is progressive. As a result, the Au layer is randomly dissolved by wet etching. In contrast, it is considered that chemical adhesion of PS resist layer to the substrate caused by UV exposure completely suppresses random penetration of the aqueous etchant into the resist and metal interfaces. The presence of the PS graft layer caused by benzophenone photochemistry improves lateral pattern resolution of Au thin layers by wet etching.

This technique is applicable for patterning of other metal layers of Cr and Cu by selecting a trimethoxysilyl group as a reaction site to substrate surfaces with the native oxide layer [6].

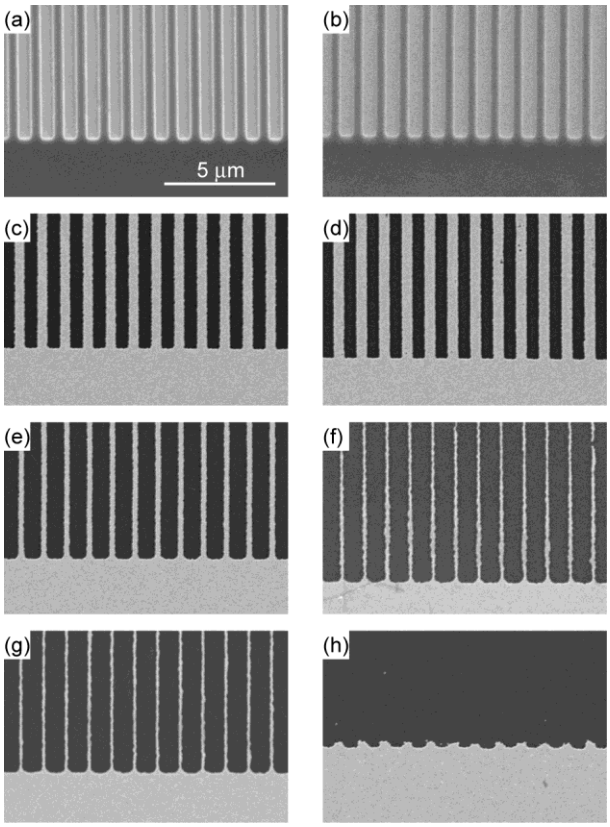

Fig. 2. SEM images of (a, b) 0.5 μm line-and-space resist layer patterns on PrM-modified Au-plated substrates after exposure to UV-light and thermal nanoimprinting and (c–h) patterned Au layers after removal of residual layers, wet etching, and removal of resist layers. The resist layers are composed of (a, c, e, g) PS and (b, d, f, h) PMMA. The periods of Au wet etching are (c, d) 30 s, (e, f) 120 s, and (g, h) 180 s.

2.2. Tuning patterned metal line width by controlled wet side-etching

In the former section, it was described that the PrM markedly contributes to fine pattern replication from a mold to a metal thin layer on a substrate by TNIL involving wet etching. Here we introduce an advanced method for decreasing line widths of patterned metal layers in a uniform manner achieved by R-TNIL [8]. Nanoimprint lithography comprises one-to-one replication processes of pressing, demolding, and dry etching. A pattern shape of a mold is replicated to a resist layer and then a substrate surface. When different pattern shapes are needed, corresponding molds should be prepared. If an identical mold is available for the fabrication of substrate surfaces with similar shapes but different sizes, the availability of TNIL will be spread. In general, with an increase in period of isotropic wet etching, line widths of metal patterns masked with a resist layer on a substrate are decreased. The side-etching occurs because isotropic wet etching proceeds not only at a vertical direction but also at a lateral direction of the metal layer. Up to date, there have been several approaches based on the side-etching to obtain nanowire structures [9-11]. We investigated what effects the PS graft layer shows in wet side-etching. Since poly(methyl methacrylate) (PMMA) is widely used as a resist material in TNIL, we compared PS with PMMA in R-TNIL involving wet etching.

Here, PS and PMMA showing an identical M_w = 35,000 g mol^{-1} were used as resist materials. Respective UV-exposed spin-coated resist layers on PrM-modified Au-plated substrates were transformed by thermal nanoimprinting using a fluorinated mold having 0.5 μm line-and-space patterns, followed by residual layer removal and Au wet etching. As shown in Figs. 2(a) and 2(b) indicating SEM images of patterned resist layers and Figs 2(c) and 2(d) indicating SEM images of Au line patterns on substrates after Au wet etching for 30 s, the Au

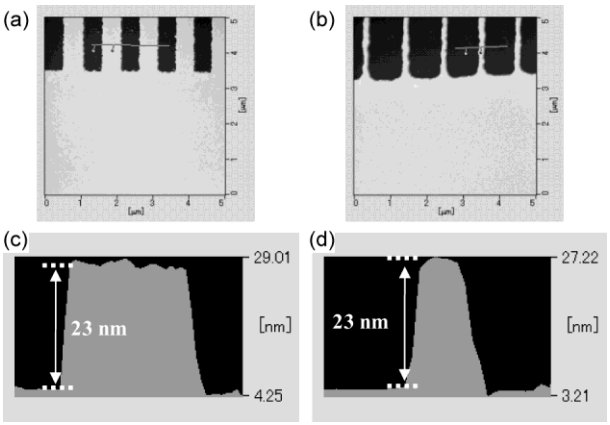

Fig. 3. (a, b) AFM images and (c, d) height profiles of Au line patterns obtained after wet etching for (a, c) 30 s and (b, d) 180 s using 0.5 μm line-and-space PS resist layer patterns.

line patterns had a line width of 0.49 μm, which was almost the same as that of resist line patterns. It is worthy to note that several pinhole defects were observed in Au lines in the case of using a PMMA resist layer as shown in Figs. 2(d). It was considered that the defect generation was attributable to resist functionality of PMMA weakened by exposure to UV light used to cause the benzophenone photochemistry and to remove a residual layer by UV/ozone. In previous reports on block copolymer lithography using PS-*block*-PMMA, PMMA regions are rapidly etched by oxygen plasma in dry etching in comparison with PS regions [12, 13]. In our study, exposure to UV/ozone is used for removal of a residual layer as a dry etching process. The PMMA resist layer is affected more than the PS resist layer. This situation results in weakened resist functionality of PMMA to aqueous etchant solutions. The formation of Au grains on surfaces of electrodeposited Au line patterns is considered to be due to the weakened resist functionality owing to degradation of PMMA by exposure to UV light [14].

With an increase in period of Au wet etching, the Au line width is decreased by the occurrence of side-etching. In the case of PS, the Au line width of 0.49 μm for an etching period of 30 s [Fig. 2(c)] decreased to 0.25 μm for 120 s [Fig. 2(e)] and 0.15 μm for 180 s [Fig. 2(f)]. Interestingly, a constant line edge roughness was maintained. In contrast, in the case of PMMA, the Au line width of 0.49 μm rapidly decreased to 0.16 μm for 120 s [Fig. 2(f)], concomitantly with an increase in line edge roughness and undercuts of Au lines. It is considered that the situation was brought about by heterogeneous side-etching. The Au lines completely disappeared after 180 s [Fig. 2(h)]. Rapid side-etching in the case of PMMA will also result from a weakened resist functionality of PMMA by exposure to UV light and UV/ozone.

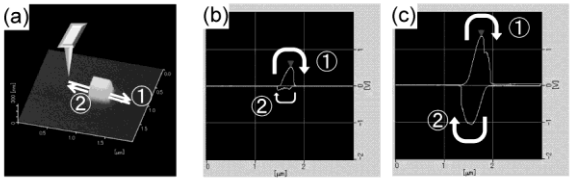

Fig. 4. (a) AFM image of single resist pattern used for collapse test with illustration of the collapse test by scanning a probe to a direction parallel to a substrate surface. Lateral force–scan length curves for UV-exposed patterns on (b) a bare silicon substrate and (c) a PrM-modified silicon substrate.

The thickness of Au line patterns after wet etching was measured using an atomic force microscope (AFM) to investigate whether side-etching changes the height. The average heights of Au lines after wet etching for 30 s [Figs. 3(a) and 3(c)] and 180 s [Figs. 3(b) and 3(d)] were almost identical to 23 nm, which agreed with the initial thickness of a Au layer before wet etching. The results indicate that the presence of the PS graft layer completely suppressed corrosion of the Au layer from a side covered with the PS graft layer within the period of wet etching for 180 s. The results from the side-etching behaviors tell us two important points. Firstly, the method of controlled wet side-etching achieved by R-TNIL provides us opportunities for tuning simply various line widths of a metal layer using single mold. Therefore, it is not necessary to fabricate various molds having different line widths. Secondly, the method is applicable to the fabrication of submicrometer patterns of metal layers at a large area from an industrial standpoint. The reason is because conventional photolithography and laser lithography faster than electron beam lithography are available for the preparation of a mold having micrometer patterns at a large area, and the micrometer patterns of the molds are reduced to submicrometer patterns of metal layers by the controlled wet side-etching. The method will reduce effectively a cost of master molds for nanoimprinting.

2.3. Mechanically enhanced adhesion of resist pattern by PrM

The direct peeling (DP) method [15] was adopted to evaluate mechanical effects of a photochemical graft reaction of the PrM on collapsing resist patterns. An illustration of the DP method to collapse a pillar resist pattern by scanning a probe reversibly at a direction parallel to a substrate

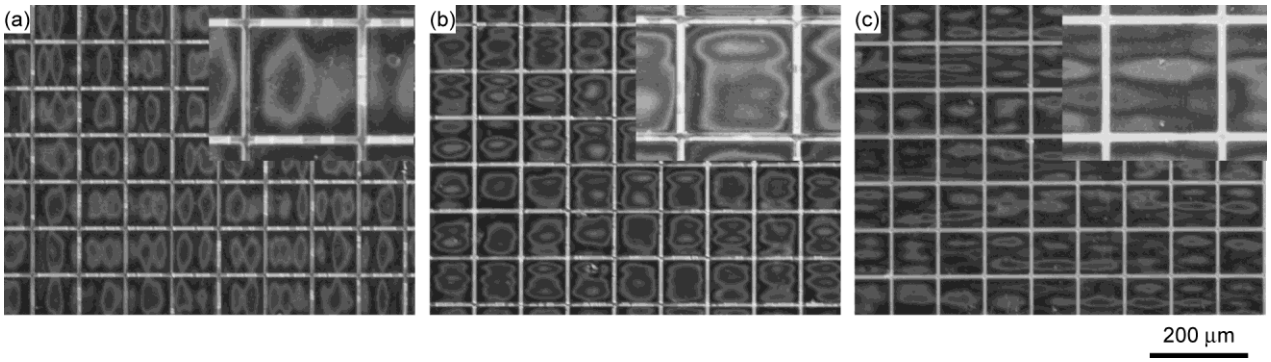

Fig. 5. Fluorescence microscope images of fluorescent dye-doped PS thin films transformed with a fluorinated Ni mold having 95 μm convex lattice squares with a 100 μm pitch by applying pressures of (a) 3.3, (b) 6.7, and (c) 12.2 MPa.

surface is shown in Fig. 4(a) with an actual AFM image of a pillar pattern used for the measurment.

A cleaned silicon substrate was subjected to chemical vapor surface modification (CVSM) to form a PrM from 4-[[(3-trimethoxysilyl)propyl]-oxy]benzophenone as described in a previous report [16]. A spin-coated thin film of an acrylate-type UV-curable resin (Toyo Gosei PAK-01) was transformed using a fluorinated silica mold having 0.5 μm square pillar patterns under a condensable gas of pentafluoropropane (PFP) and cured by exposure to UV light at irradiation wavelengths of >360 nm in a manner silimar to previous reports [17, 18]. After demolding, cured resin patterns were exposed again to UV light at an exposure energy of 2.0 J cm^{-2} monitored at 254 nm. After inducing the benzophenone photochemistry, the residual layers were removed by exposure to vacuum ultraviolet light emitted at 172 nm. Thus obtained pillar patterns were peeled from the silicon substrate by a cantilever (Olympus AC-200TS) using a scanning probe microscape (SII S-image). Lateral forces were detected when the probing tip was moved across single pillar pattern. The probing tip without vibration at a constant distance of 30 nm from the substrate surface was scanned reversibly at a direction parallel to the substrate surface.

Figures 4(b) and 4(c) show lateral force–scan curves for a pillar prepared on a bare silicon surface and a pillar grafted on a PrM-modified silicon surface, respectively. When the pillar just stood on the substrate surface, an increase in lateral force was detected once at a forward direction. The pillar was peeled off from the silicon surface and was not left when the cantilever moved backward. To the contrary, an increase in lateral force was detected at both of forward and backward directions in the case of the pillar grafted on the PrM-modified substrate surface. The pillar was still left without collapse after the cantilever was scanned. These results suggested that the grafted pillar pattern was strongly anchored covalently by the benzophenone photochemistry that the PrM caused by exposure to UV light at 254 nm [19].

3. Transparent conductive substrates having metal mesh structures

Transparent conductive substrates are very important components for touch panel screens, display devices, solar cells, and so on [20]. Instead of conventional transparent conductive substrates coated with indium-tin-oxide (ITO), transparent conductive substrates having a mesh structure made with noble metals is promising because of reducing fabrication costs and decreasing use of rare metals. Metal mesh structures are mainly fabricated by screen printing and ink-jet printing using paste inks containing metal fillers. The line widths are limited to larger widths than several tens of micrometers. More sophisticated methodologies matched to industrial requirement for the fabrication of micrometer and submicrometer metal patterns in cost-effective and high-throughput ways should be developed. Here we introduce R-TNIL involving wet etching and side-etching as a promising way to prepare transparent conductive substrates having metal mesh structures.

A Ag/PEN sheet having a Ag layer of 0.12 μm in thickness on a poly(ethylene naphthalate) film was used for a substrate, and a benzophenone-containing PrM was formed on the Ag layer as shown previously [5]. A fluorescent dye-doped PS resist layer was prepared by spin coating for resist pattern inspection [21]. *N*,*N*'-Bis(2,6-dimethylphenyl) perylene-3,4,9,10-tetracarboxylic diimide was used as the fluorescent dye. The PS resist layer was transformed using a fluorinated Ni mold having 95-μm square convex lattice patterns with 5 μm concave lines. Figures 5(a–c) show fluorescence microscope images of transformed resist layers by applying pressures of 3.3, 6.7, and 12.2 MPa, respectively. The fluorescence intensity qualitatively

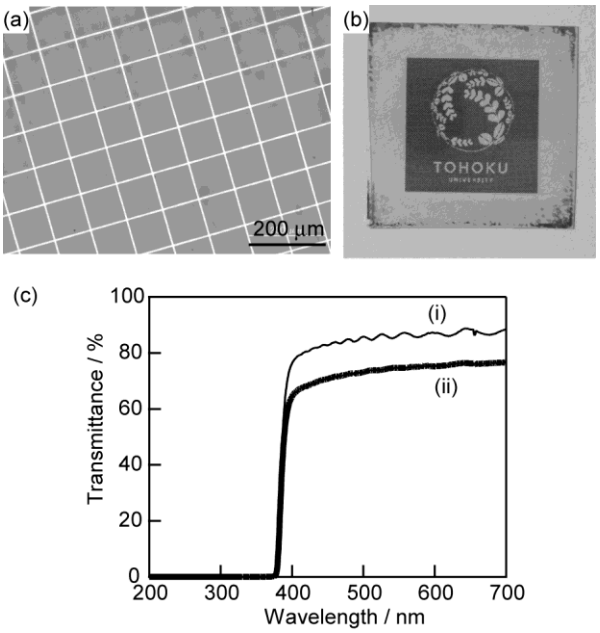

Fig. 6. (a) Optical microscope image and (b) photograph of a PEN sheet with a Ag mesh structure which had a Ag line width of 5 μm at a pitch of 100 μm. (c) UV-visible transmission spectra of PEN sheets (i) without and (ii) with the Ag mesh structure.

corresponds to the thickness of the dye-doped PS resist layer. The darker squares and brighter lines indicated that the PS resist layers were transformed to mesh structures. It was clearly observed that the PS resist layers transformed under pressures of 3.3 and 6.7 MPa had partial filling defects, while the resist layer pressed at 12.2 MPa had no significant defects. Thus, the fluorescence images observed by fluorescence microscopy allow quick inspection to look for defects that are difficult to observe by bright field optical microscopy.

A Ag mesh structure on a PEN sheet was obtained after removal of residual layers formed at square regions by exposure to UV/ozone and subsequent wet etching of Ag. Figure 6(a) shows an optical microscope image of obtained Ag mesh structure. The Ag mesh structure on a 3-cm square PEN sheet looks transparent as shown in Fig. 6(b). The UV-visible transmission spectrum of a PEN sheet having the Ag mesh structure is shown in Fig. 6(c) with the spectrum of a PEN sheet as a reference. The average transmittance of the Ag mesh structure was 87 % to the PEN sheet in a wavelength region of 400 – 700 nm. The surface resistivity of the Ag mesh structure was 20 Ω/square, indicating that the Ag mesh maintained electrical conductivity. This method of R-TNIL involving wet etching is not dependent on the kind of substrate and metal in principle. Ag and Au mesh structures on fused silica substrates could be also fabricated in the same manner [22, 23].

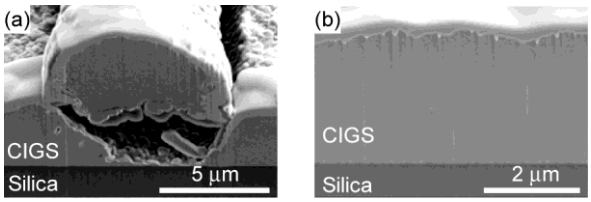

Fig. 7. Cross sectional SEM images of a CIGS multilayer film formed on a Ag mesh/silica substrate. (a) The CIGS multilayer was exfoliated. (b) The Ag lines were lost during formation of the CIGS multilayer.

We investigated whether the Ag mesh/silica substrate was available for a substrate to form a Cu-In-Ga-Se (CIGS) multilayer applicable to photovoltaic devices. On the Ag mesh/silica substrate, a 1 μm-thick Al-doped zinc oxide (AZO) layer, a 50 nm-thick ZnO layer, and a 50 nm-thick CdS layer were prepared, and a 2 μm-thick CIGS multilayer was finally deposited by vacuum sputtering at 550 ºC. The Ag mesh structures were exfoliated from a substrate surface as shown in Fig. 7(a) and partially lost from the substrate surface as shown in Fig. 7(b). It was considered that the Ag exfoliation is derived from weak adhesion of Ag on a substrate surface in addition to a difference in thermal expansion between silica and Ag, and that the loss of Ag is due to migration of Ag to the CIGS multilayer. It seemed that the transparent conductive substrate with metal mesh structure will be suitable for use around room temperatures.

4. Fine Au electrodeposition assisted by PrM

A subtractive method of wet etching has limitations to the thickness of a metal layer and the morphology of fabricated metal patterns. In particular, side walls of patterned metal layers are tilted, and it is difficult to fabricate patterned metal layers with tuned aspect ratios. This is because wet etching occurs in an isotropic manner. We investigated R-TNIL involving Au electrodeposition and subsequent etching for the fabrication of Au patterns applicable to optical devices [24].

A UV-exposed PS resist layer on a PrM-modifed Au-plated substrate was thermally transformed to 0.2 μm line-and-space patterns. After removal of residual layers, Au electrodeposition was carried out using the Au substrate masked with the patterned PS resist layer as a working electrode in a similar manner described in a previous report [14]. Figure 8 shows a tilted SEM image of an electrodeposited Au pattern. Fine line-and-space Au patterns having a height of approximately 0.15 μm could be prepared. Electrodeposited Au grew only at aperture regions without PS resist masks, and the growth of Au grains at masked regions were hardly observed. In

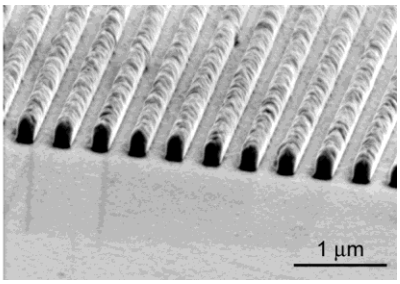

Fig. 8. SEM image of electrodeposited Au patterns of 0.2 μm line-and-space.

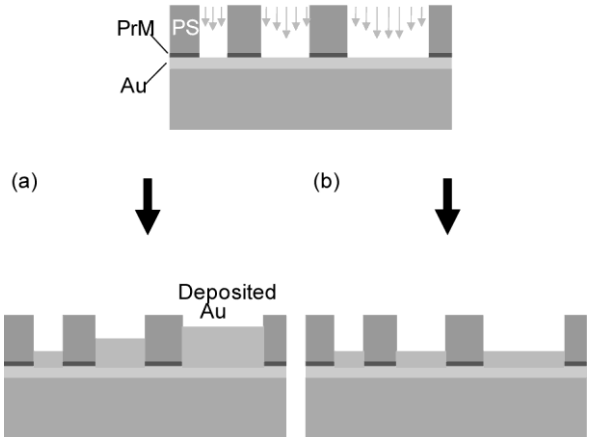

Fig. 9. Schematic illustrations of Au electrodeposition at convex regions of resist patterns having different aperture sizes at (a) a high current density and (b) a low current density.

contrast, a lot of Au grains with sizes of several tens of nanometers grew in the case of PS resist mask formed on a bare Au surface [14] and on an unexposed PrM-modified Au surface [24]. It is worthy to note that the presence of a PS graft layer formed by a benzopehnone-containing PrM upon exposure to UV light suppresses undesired growth of Au grains at regions masked with PS resist layers. The suppressive effect on the growth of tiny Au grains was dependent on a molecular weight of monodisperse PS used as resist materials. The detail will be published [24].

The height of electrodeposited Au lines could be controlled simply by changing periods of electrodeposition at a low current density. However, with an increase in current density, the height was uncontrollable at aperture line widths smaller than 0.2 μm. The results indicate that the Au electrodeposition is a diffusion-limit reaction. The diffusion of electro-active Au ion species might be suppressed at aperture regions of a line width smaller than 0.2 μm at a high current density. As a result, the heights of Au lines did not become uniform as illustrated in Fig. 9(a). It was found that a decrease in current density was necessary to obtain Au

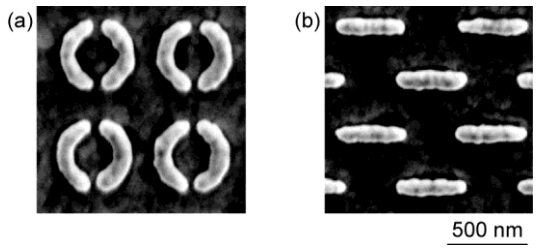

Fig. 10. SEM images of (a) Au sprit ring patterns having a metal width of 125 nm and two gaps of 20 nm and (b) Au nanorods having a width of 100 nm and a length of 500 nm fabricated by R-TNIL involving Au electrodeposition.

lines with a uniform height independent of aperture sizes as shown in Fig. 9(b). We demonstrated that Au line bump structures could be fabricated by R-TNIL involving Au electrodeposition and subsequent wet etching of Au and Cr layers used as an electrode [24].

Also we have recently fabricated Au sprit ring patterns having a metal width of 125 nm and two gaps of 20 nm as shown in Fig. 10 (a) and Au nanorods having a width of 100 nm and a length of 500 nm as shown in Fig. 10 (b). The fine Au nanostructure patterns could be obtained at an entire area of 100 μm square [25]. R-TNIL using a PrM will open opportunities to fabricate metal nanostructures suitable for studies of unique optical properties that such metal nanostructures exhibit.

5. Conclusion

In this article, we reviewed the fabrication of patterned metal nanostructures on substrates by R-TNIL using a benzophenone-containing photoreactive monolayer (PrM). The PrM played important roles by anchoring a resist layer of hydrophobic and hydrocarbon thermoplastic PS covalently at the interface. The benzophenone monolayer photochemistry formed a PS graft layer, resulting in suppression of dewetting of a PS resist layer, controlled wet side-etching, and suppression of undesired growth of tiny electrodeposited Au grains at regions masked with a PS resist layer. The line widths of patterned metal layers on substrates could be reduced by controlled side etching from micrometers to submicrometers. The method allowed us to fabricate submicrometer metal patterns at a suitable throughput and at a large area without dependence on EB lithography and advanced photolithography. Applicability of R-TNIL to practical use was shown by demonstrating the fabrication of transparent conductive substrates having metal mesh structures. In addition, we demonstrated that R-TNIL using a PrM was applicable to metal electrodeposition to obtain various

metal nanostructures with controlled height. Considering potentials for mass production, R-TNIL will become a powerful tool to fabricate innovative electrical, optical, and magnetic devices comprising metal nanostructures.

Acknowledgement

This work was supported in part by KAKENHI (20350103) Grant-in-Aid for Scientific Research (B), KAKENHI (22108502) Grant-in-Aid for Scientific Research of Innovative Areas, and the Management Expenses Grants for National Universities Corporations from the Ministry of Education, Culture, Sports, Science and Technology of Japan (MEXT). The authors thank NOF CORPORATION and Asahi Kasei E-materials Corp. for their financial supports in Joint Researches and DNP for his supply of silica and silicon nanoimprint molds. We thank Prof. K. Yoshino and his group members for cooperation in fabrication of CIGS multilayers. We also thank Dr. H. Oda, Dr. K. Kobayashi, Dr. K. Nagase, and Mr. T. Tomioka of Tohoku University for their experiments.

References

1. S. Y. Chou, P. R. Krauss, and P. J. Renstrom, *Appl. Phys. Lett.* **67** (1995) 3114.
2. J. Haisma, M. Verheijen, K. van den Heuvel, and J. van den Berg, *J. Vac. Sci. Technol. B* **14** (1996) 4124.
3. S. Matsui, Y. Igaku, H. Ishigaki, J. Fujita, M. Ishida, Y. Ochiai, M. Komuro, and H. Hiroshima, *J. Vac. Sci. Technol. B* **19** (2001) 2801.
4. Y. Igaku, S. Matsui, H. Ishigaki, J. Fujita, M. Ishida, Y. Ochiai, H. Namatsu, M. Komuro, and H. Hiroshima, *Jpn. J. Appl. Phys.* **41** (2002) 4198.
5. H. Oda, T. Ohtake, T. Takaoka, and M. Nakagawa, *Langmuir* **25** (2009) 6604.
6. S. Kubo, T. Ohtake, E.-C. Kang, and M. Nakagawa, *J. Photopolym. Sci. Technol.* **23** (2010) 83.
7. H. Oda, T. Ohtake, T. Takaoka, and M. Nakagawa, *J. Photopolym. Sci. Technol.* **22** (2009) 195.
8. M. Nakagawa, K. Nagase, and S. Kubo, Jpn. Pat. Appl. 2011-207444 (2011).
9. E. J. Menke, M. A. Thompson, C. Xiang, L. C. Yang, and R. M. Penner, *Nat. Mater.* **5** (2006) 914.
10. Y. Yang, D. K. Taggart, M. A. Brown, C. Xiang, S.-C. Kung, F. Yang, J. C. Hemminger, and R. M. Penner, *ACS Nano* **3** (2009) 4144.
11. C. Xiang, S.-C. Kung, D. K. Taggart, F. Yang, M. A. Thompson, A. G. Güell, Y. Yang, and R. M. Penner, *ACS Nano* **2** (2008) 1939.
12. K. Asakawa and T. Hiraoka, *Jpn. J. Appl. Phys.* **41** (2002) 6112.
13. Y.-H. Ting, S.-M. Park, C.-C. Liu, X. Liu, F. J. Himpsel, P. F. Nealey, and A. E. Wendt, *J. Vac. Sci. Technol. B* **26** (2008) 1684.
14. K. Nagase, S. Kubo, and M. Nakagawa, *Jpn. J. Appl. Phys.* **49** (2010) 06GL05.
15. M. Kurihara, S. Hatakeyama, K. Yoshida, M. Abe, D. Totsukawa, Y. Morikawa, H. Mohri, M. Hoga, N. Hayashi, H. Ohtani, and M. Fujihira, *Jpn. J. Appl. Phys.* **48** (2009) 06FG01.
16. S. Kubo and M. Nakagawa, *Jpn. J. Appl. Phys.* **49** (2010) 06GL03.
17. H. Hiroshima and M. Komuro, *J. Vac. Sci. Technol. B* **25** (2007) 2333.
18. H. Hiroshima and M. Komuro, *Jpn. J. Appl. Phys.* **46** (2007) 6391.
19. K. Kobayashi, M. Kurihara, M. Hoga, S. Matsui, and M. Nakagawa, *The 71st Autumn Meeting of the Jpn. Soc. Appl. Phys.* (2010) 15p-K-6.
20. L. Hu, H. Wu, and Y. Cui, *MRS Bulletin* **36** (2011) 760.
21. S. Kubo, Y. Sato, Y. Hirai, and M. Nakagawa, *Jpn. J. Appl. Phys.* **50** (2011) 06GK10.
22. S. Kubo, K. Nagase and M. Nakagawa, *Chem. Lett.* in press.
23. S. Kubo, K. Nagase, T. Ohtake, E.-C. Kang, H. Kataoka, T. Yamada, K. Nagase, and M. Nakagawa, *Polymer Preprints* **60** (2011) 5609.
24. K. Nagase, S. Kubo, and M. Nakagawa, *Langmuir* in press (DOI: 10.1021/la301632y).
25. T. Tomioka, K. Nagase, S. Kubo, M. Houga, and M. Nakagawa, *The 59th Spring Meeting of the Jpn. Soc. Appl. Phys.* (2011) 18p-A2-8.